Journal of
Nanoscience and Nanotechnology
Vol. 8, 1–7, 2008

Nanocrystalline CdSe Thin Films of Different Morphologies in Thermal Evaporation Process

U. Pal[1,*], M. Herrera Zaldivar[2], R. Sathyamoorthy[3], V. Manjuladevi[3], P. Sudhagar[3], S. Chandra Mohan[3], and S. Senthilarasu[3]

[1] *Instituto de Física, Universidad Autónoma de Puebla, Apdo. Postal J-48, Puebla, Pue. 72570, Mexico*
[2] *Centro de Ciencias de Materiales Condensada, Universidad Nacional Autónoma de México, Apdo. Postal. 2681, Ensenada, BC 22800, Mexico*
[3] *Department of Physics, Kongunadu Arts and Science College, Coimbatore, India*

Cadmium selenide nanocrystalline thin films of quasi-spherical morphology are prepared by evaporating CdSe nanopowders on glass substrates. Slightly oval shaped CdSe particles of about 165 nm average size (in 2-D) could be assembled over glass substrates by controlling the film thickness. Morphologies like assembly of particles, interconnected particles with mosaic-like structures and thin films of smooth surfaces could be prepared simply by controlling film thickness. A mechanism for such morphological variations is proposed. Observed variation of band gap energy in the films is explained in terms of quantum confinement effect and substrate-film interface strain.

Keywords: Nanocrystalline, CdSe Thin Films, Morphology, Optical Properties.

RESEARCH ARTICLE

1. INTRODUCTION

Inorganic nanostructures in the forms of dots, tubes and wires exhibit a wide range of electrical and optical properties[1,2] depending sensibly on their size and shape,[3,4] which are of both fundamental and technological interests. The II–VI semiconductor systems have many applications such as light emitting diodes and biological sensors.[5–7] Cadmium selenide (CdSe) is one of the most important II–VI semiconductors with promising optoelectronic applications, especially in nanoscale where the nonlinear optical and quantum size effects[8] are in vogue. The band gap of CdSe nanostructures can be tuned across the visible spectral region by tuning their sizes. Due to this particular property CdSe has attracted great attention as optoelectronic material. CdSe nanoparticles in pure or hybrid structures like CdSe-core/ZnS-shell are presently being investigated for their applications in biological imaging and fluorescence detection.[9,10] However, most of the synthesis efforts are confined to their colloidal forms through chemical routs. The physical methods like MBE (molecular beam epitaxy),[11] MOCVD (metal organic vapor chemical deposition),[12] OMVPE (organo metallic vapor phase epitaxy),[13] thermal evaporation,[14] and chemical techniques like solvothermal,[15] hydrothermal,[16] surfactant-assisted chemical synthesis[17] were used for the preparation of CdSe nanostructures. Synthesis of morphology controlled CdSe nanostructures through any of the physical or chemical methods is extremely important for their technological applications.

In the present article, we report on the deposition of CdSe thin films with controlled surface morphology simply by evaporating CdSe nano-powders on glass substrates. By controlling the thickness of the deposits, array of nanoparticles, mosaic-like structures and continuous thin films could be prepared. Techniques like X-ray diffraction (XRD), scanning electron microscopy (SEM), and optical absorption spectroscopy are used to characterize the nanostructures. Observed charge carrier confinement and valence band splitting in the nanostructured films are discussed. A mechanism for the variation of morphology with film thickness is proposed.

2. EXPERIMENTAL DETAILS

2.1. Synthesis of CdSe Powders

The CdSe nanopowders are prepared through a surfactant-assisted chemical technique.[18] All chemicals used in this work are purchased from Fluka and Merck and were of analytical grade. For the synthesis of CdSe nanopowders, CdO (100 mM) and Triton 100 X (∼24 mM) were loaded into a round bottom flask and heated at 40 °C. Solution of sodium hydrogen selenide ($NaBH_4$/Se in 40 ml water) was

*Author to whom correspondence should be addressed.

added to the mixture drop-wise under constant stirring. The resulting mixture was refluxed for 12 h (at 40 °C) and left overnight. The product was washed repeatedly with cyclohexane and diethyl ether to remove the surfactant, and decanted with acetone to obtain fine powders.

2.2. Preparation of CdSe Nanocrystalline Films

Cadmium selenide nanopowders prepared by the above mentioned procedure were taken as the source material for thermal evaporation. The powders were placed in a molybdenum boat (200 amps) and heated with high current through an energizing transformer. The transformer capable of supplying 150 amperes at 20 Volts was used to provide the necessary current for heating the molybdenum boat. Prior to evaporation, the CdSe powder material was carefully degassed at a lower temperature for about 30 min with the shutter closed. Deposition of the material on to pre-cleaned glass substrates under the pressure of about 10^{-5} Torr was achieved by slowly varying the heating current. A constant rate of evaporation 1 Å/S was maintained throughout the film preparation. The substrate to source distance was kept at 17.9 cm inside the vacuum chamber. The thickness of the deposited films was monitored using a quartz crystal monitor. Thin films of 67, 170 and 305 nm thickness were prepared by controlling the time of deposition.

Crystalline structure of the films was characterized by XRD (Phillips X'Pert diffractometer) using CuK_α ($\lambda = 1.5406$ Å) radiation. The surface morphology and composition of the films were studied using a scanning electron microscope (SEM, JEOL JSM-5300) with Thermo Noran SuperDry II analyzer. As the thicknesses of the films were very small, the energy dispersive spectra (EDS) of the films were recorded by tilting the films at 55° with respect to the incident electron beam. Optical absorption spectra of the thin films were recorded through a SHIMADZU 3101PC UV-VIS-NIR spectrophotometer using a clean glass substrate as reference. A JEOL JSPM 5200 nanoscope operating in contact mode was used for the topological study of the film surfaces.

3. RESULTS AND DISCUSSION

3.1. X-ray Diffraction

The XRD patterns of nanocrystalline CdSe thin films of different thickness are shown in Figure 1. All the films prepared by present method are nanocrystalline in nature with predominant hexagonal (wurtzite) phase. Similar background intensity and well defined peak positions in the films demonstrate the broad background comes from the amorphous glass substrate. With the increase of film thickness, the intensity of the diffraction peaks increased initially and then remained unchanged. Though the EDS results revealed a drastic deviation of stoichiometry in thinner films (Table I), the XRD results demonstrate the presence of small amount of excess Se in all the samples, irrespective of their thickness. Such a deviation of stoichiometry is expected as the films were grown at room temperature. Apart from the peaks correspond to the predominant hexagonal phase, the XRD spectra revealed peaks of cubic phase CdSe in the samples. The average crystallite size of the films was calculated for the peak (100), common for all the samples, by using the Scherer formula:

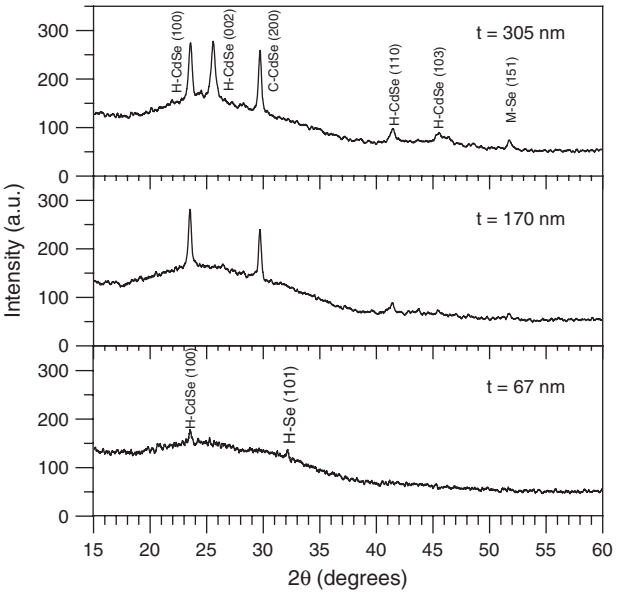

Fig. 1. XRD patterns of CdSe nanocrystalline thin films of different thicknesses. *H*, *C* and *M* stand for hexagonal, cubic and monoclinic respectively.

$$D = 0.94\lambda/\beta\cos\theta$$

where D is the crystallite size, λ is the X-ray wavelength (1.5406 Å), β is the angular full width at half maximum (FWHM) of intensity, and θ is the Bragg angle. As the intensity of the diffraction peaks was low, we used Gaussian fits to the peaks to extract corresponding FWHM and peak positions. The peak positions and estimated average particle/grain sizes of the films are presented in Table I. It must be noted that though the diffraction peak intensity in the films increased, the average particle size of the films evaluated from XRD decreased with the increase of their thickness. The probable reason for such a decrease of average particle size with film thickness is discussed latter.

3.2. Electron Microscopy

In Figures 2–4, SEM micrographs of the thin films of different thicknesses are presented at different magnifications. In Figure 2, we can observe a homogeneous distribution of nanometer size particles. The oval shape of the particles can be observed easily in high magnification micrographs. The planer (2-D) size distribution of the

Table I. Composition, structural and optical parameters of nanocrystalline CdSe films of different thicknesses.

Film thickness (nm)	Se/Cd atomic ratio	XRD peak positions, 2θ (degrees)	d (Å) experimental	d (Å) standard	hkl	Particle size D (nm)	Band gap E_g (eV)	
							E_g^1	E_g^2
67	1.8	23.54	3.776	3.723	100	52.3 ± 3	2.37	2.67
170	1.7	23.52	3.780	3.723	100	49.3 ± 3	2.15	2.38
		29.70	3.006	3.039	*C*-200			
305	1.1	23.56	3.773	3.723	100	39.6 ± 4	1.95	2.25
		25.60	3.477	3.505	002			
		29.68	3.008	3.039	*C*-200			

oval shaped particles is shown in the histogram (Fig. 2). We can see that the particles are more or less homogeneous in size with average of about 165 nm and about 20% dispersion (from the Gaussian fit of the histogram). As the thickness of the film was about 67 nm, the 165 nm planer average size indicates the particles are flat with plate like morphology. Their vertical thickness (or height in Z-direction) must be much less than their planer dimensions. In fact, such a flat morphology of the particles is confirmed through atomic force microscopic (AFM) studies of the sample (discussed latter). Although, the disagreement between particle sizes measured by XRD and SEM is known and quite common,[19] which is most probably due to agglomeration of small particles into larger aggregates, the particle size of the film estimated from XRD (52.3 nm) is quite small. Such a vast difference in estimated particle size by the two techniques is mainly due to the flat or disk like morphology of particles formed on the glass substrate.

From the SEM images of the 170 nm thick film presented in Figure 3, we can observe a mosaic like morphology generated by interconnecting the oval-shaped particle observed in the earlier sample.

On further increasing the film thickness, the mosaic-like morphology disappears and almost a continuous film with smooth surface morphology is formed. In the micrograph (a) of the Figure 4, we can still observe a few particles

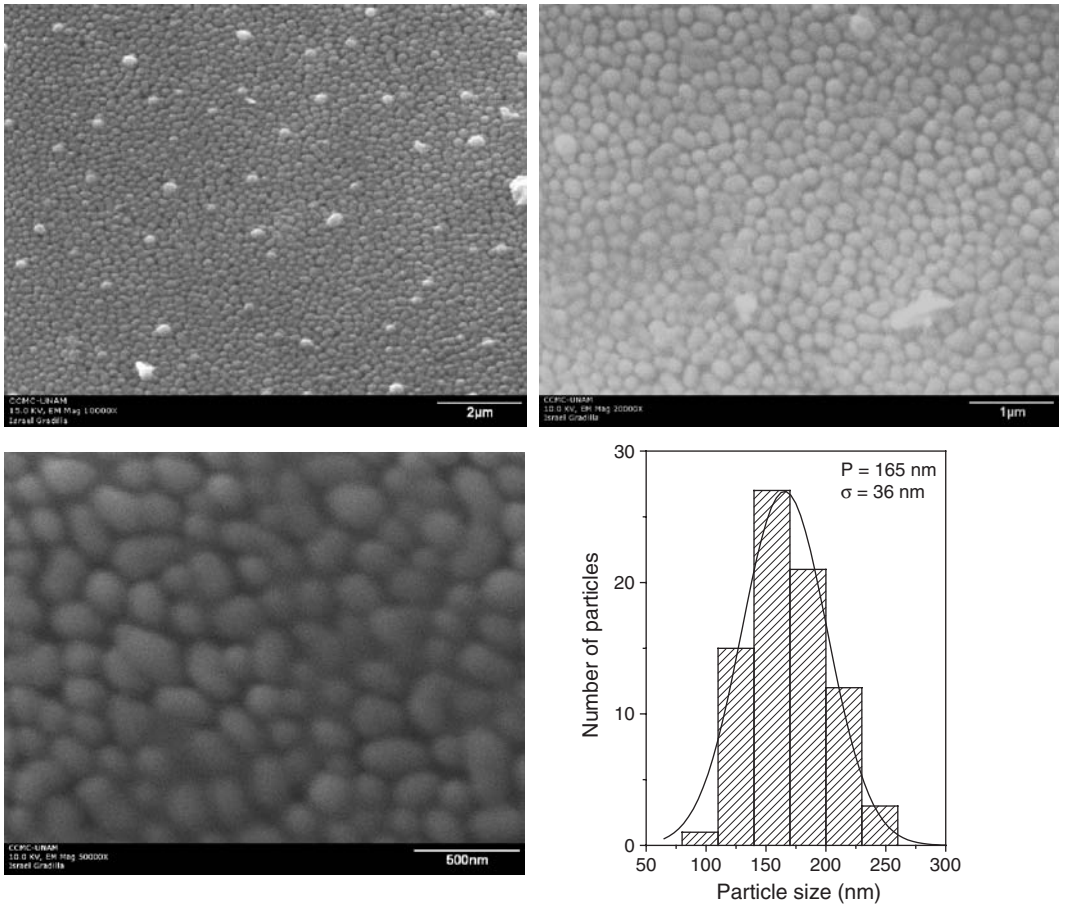

Fig. 2. SEM micrographs of as-deposited CdSe film of thickness 67 nm along with size distribution histogram.

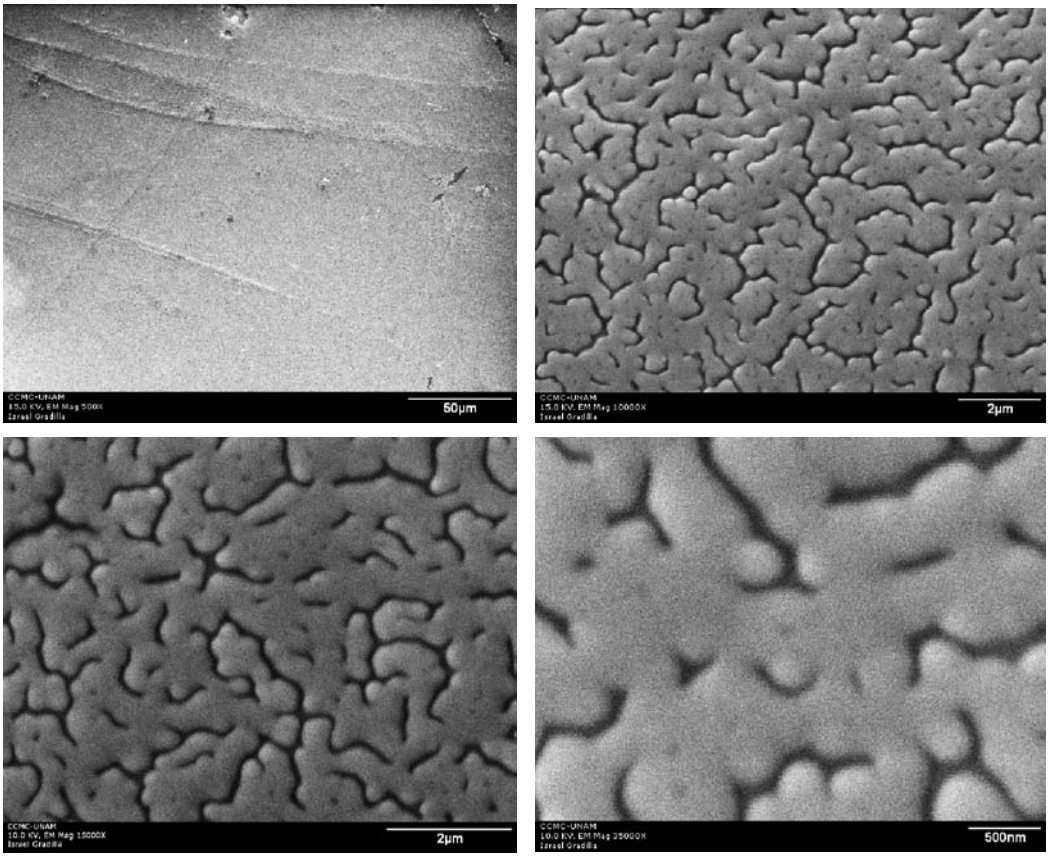

Fig. 3. SEM micrographs of as-deposited CdSe film of 170 nm thickness at different magnifications. Interconnected particles or particles in agglomeration can be seen in the micrographs.

almost immersed in the film. At this stage, some needle like nanostructures were formed on the film surface, especially at the artifact sites (Fig. 4(b)). Effect of surface artifacts on the formation of these linear nanostructures is clear from the Figure 4(c), where we can observe the formation of needle-like nanostructures around a crack site.

To verify the non-spherical shape of the nanoparticles in the film of thickness 67 nm, we performed atomic force microscopy (AFM) imaging of the sample. In Figure 5, typical planer and 3-D views of a 1.6 μm $\times$ 1.0 μm surface are shown. While the planer dimension of the particles can be estimated from the Figure 5(a), the height of the particles which is clearly very small in comparison with their length or width, can be estimated from the Figure 5(b). The thickness/height of the particles varied from 11 to 60 nm, with estimated average of about 30 nm. Therefore, the particles assembled on the film surface are really flat with oval shape in X–Y plane (parallel to the substrate surface). It must be noted that the average particle size for the sample estimated from (100) XRD peak is about 52 nm, which is higher than the average thickness of the particles, but very much lower than their lateral dimensions estimated from AFM.

In Figure 6, a schematic representation of the film growth mechanism generating different morphologies, as observed in our experiments is shown. While in stages (a and b), nucleation and growth of particles occur due to the condensation of incoming vapor, in stage (c), condensation of incoming vapor fills up the inter-particle spaces along with the growth of the particles, to some extent. Fusion/agglomeration of the particles on the substrate surface produces mosaic-like morphology of the film. Further condensation of the incoming vapor on the film surface results the formation of continuous film (stage d). According to our growth model, though the size of the initially nucleated particles grows to some extent, continuous formation of new particles of smaller sizes on increasing the film thickness causes a net decrease of average particle size, in agreement with the XRD results (Table I). Absence of plenty particulate structures on the surface of thicker films as revealed in their SEM micrographs (Fig. 4), also vindicate the above reasoning.

3.3. Optical Properties

Optical absorption spectra of the thin films were recorded in the 200–1000 nm spectral range at room temperature using a clean glass substrate as reference. Absorption coefficient α was determined at each wavelength using the thickness of the corresponding thin films.

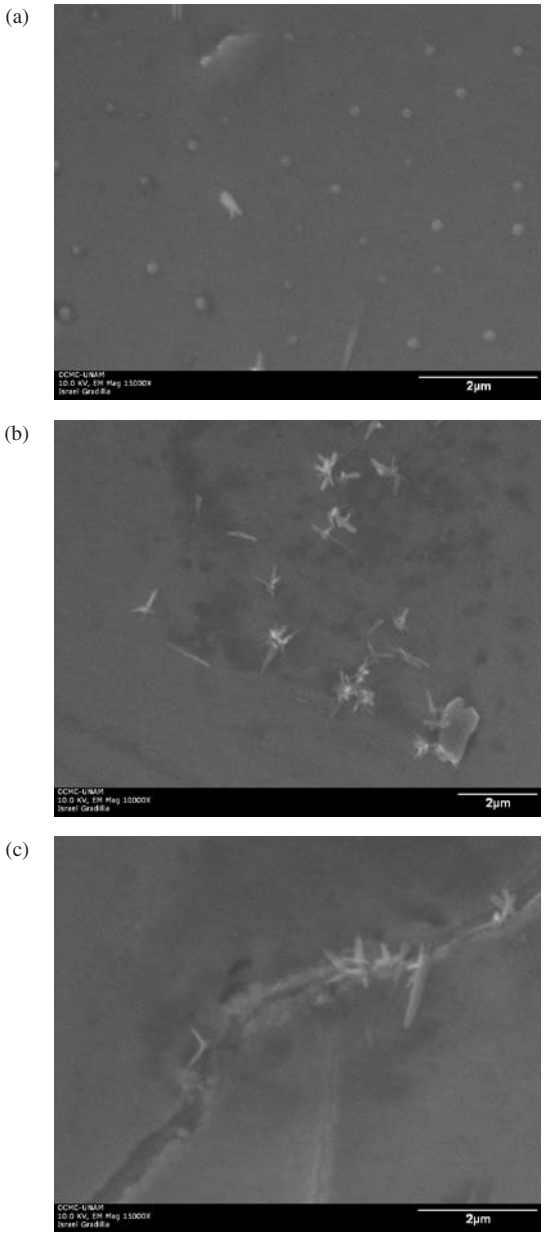

Fig. 4. SEM micrographs of as-deposited CdSe film of 305 nm thickness at different sites. While a few small particles can be seen in (a), needle like nanostructures and their formation at crack site can be seen in (b) and (c) respectively.

The band gaps 'E_g' of the samples were calculated using the relation:

$$\alpha h\nu = A(h\nu - E_g)^n$$

where $h\nu$ is the photon energy and A, n are constants. For allowed direct transitions $n = 1/2$. From the $(\alpha h\nu)^2$ versus $h\nu$ plots presented in Figure 7, the direct band gap of the samples were determined.

From the linear fits, we could extract two direct band gap values for each of the films which are designated as E_g^1 and E_g^2 and presented in Table I. As the difference between these two gaps is about 30 meV, we believe, the origin

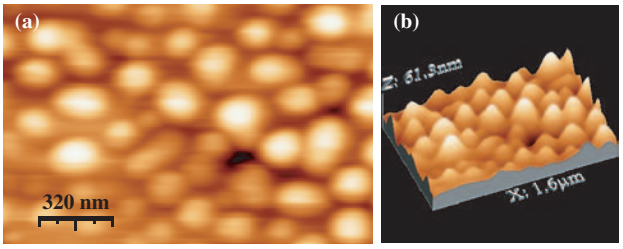

Fig. 5. Typical AFM image of the CdSe film of 67 nm thickness; (a) top view and (b) 3D representation of an area 1.6 μm × 1.0 μm. Ordered assembly of oval shaped particles (in X–Y plane) (Fig. a) of thickness ranging from 11 nm–60 nm can be seen (Fig. b).

of two direct band gap values is the spin-orbit splitting of valance band of CdSe, as observed previously.[20, 21] Estimated values of both the gaps (E_g^1 and E_g^2) are substantially higher than the bang gap value of bulk CdSe (1.74 eV). The E_g^2 values varied from 2.67 eV to 2.26 eV as the CdSe film thickness increased from 67 nm to 305 nm. As the average particle/crystallite size in our CdSe films estimated from XRD analysis were in the 39–52 nm range and the excitonic Bohr radius of CdSe is about 5.6 nm,[22] possibility of charge carrier confinement in them is very less. However, as the particles in our samples are not spherical (as demonstrated through AFM imaging) and their vertical thickness varies from 11–60 nm, a week quantum confinement of charge carriers might be in effect only in the

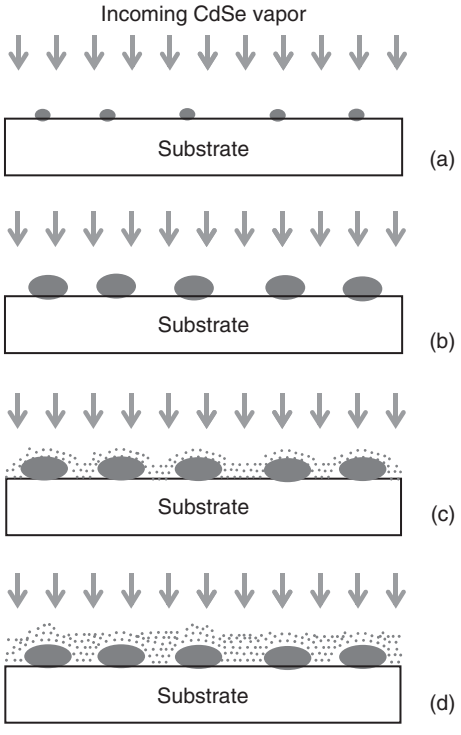

Fig. 6. Schematic representation of CdSe film growth mechanism at different stages: (a) nucleation on the glass substrate, (b) growth of oval shaped particles, (c) particle growth along with filling of inter-particle spaces, (d) continuous film formation.

RESEARCH ARTICLE

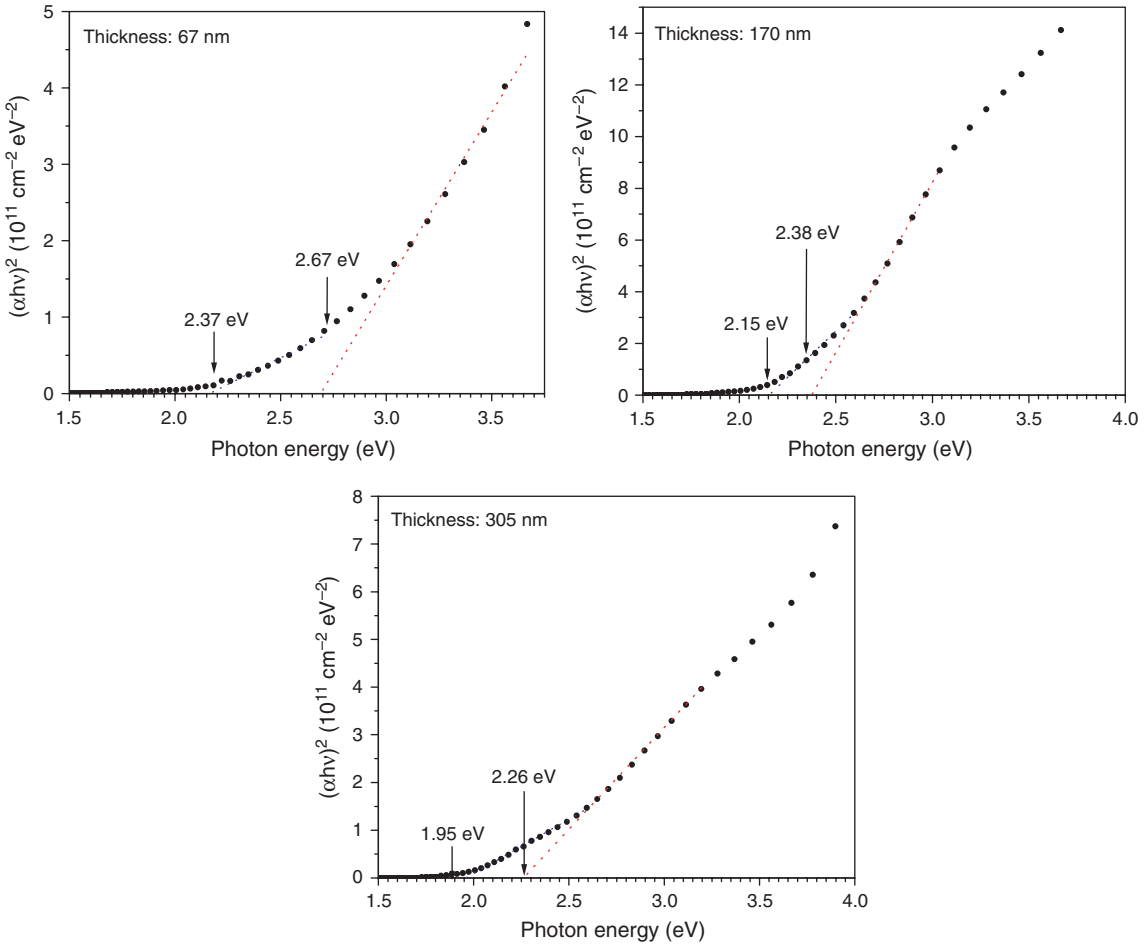

Fig. 7. $(\alpha h\nu)^2$ versus $h\nu$ plots for nanocrystalline CdSe thin films of different thickness.

particles of smaller heights. On the other hand, as the band gap of Se (1.5 eV) is lower than CdSe (1.74 eV), presence of excess Se in our CdSe films (Table I) can not cause any blue shift of band gap. Therefore, we designate the observed blue shift of band gap in our samples mainly to the residual strain at the film-substrate interface[21, 23] and to some extent to the quantum confinement effect in flat particles of smaller thickness.[24–26] As the thickness of the films increases the film-substrate interface strain decreases.

4. CONCLUSIONS

Nanocrystalline CdSe thin films of different morphologies could be prepared by evaporating CdSe nanopowders. Simply by controlling the thickness, thin films with assembly of nanoparticles, mosaic-like structures and continuous films of smooth surface morphology could be prepared in well controlled manner. The particles in the films are flat with oval shape in planer views and of a few nanometers in vertical thickness. Due to spin-orbit splitting of valence band, two direct band gaps could be estimated for the films. The blue shift of band gap energy in the films is mainly due to the film-substrate interfacial strain. As the interface strain of the films decreased with thickness, their band gap energy decreased. A possible mechanism for the growth of CdSe thin films with different morphologies is discussed. To our knowledge, this is the first time we demonstrate the preparation of nanocrystalline CdSe thin films with different morphologies in a controlled manner, using a simple thermal evaporation process.

Acknowledgments: The authors wish to acknowledge the Secretary and the management of Kongunadu Arts and Science College for their support to carry out this work. One of the author (R. Sathyamoorthy) wish to acknowledge the University grants commission, New Delhi for awarding UGC research award. U. Pal acknowledges the partial financial help of CONACyT, Mexico (Grant No. 46269). We are thankful to E. Aparicio Ceja, CCMC-UNAM for her help in recording XRD spectra of the samples.

References and Notes

1. J. M. Heath, *Acc. Chem. Res.* 32, 389 (**1999**).
2. A. P. Alivisatos, *Science* 271, 933 (**1996**).
3. C. M. Lieber, *Solid St. Commun.* 107, 607 (**1998**).

4. R. E. Smalley and B. I. Yakobson, *Solid St. Commun.* 107, 597 **(1998)**.
5. V. L. Colvin, M. C. Schlamp, and A. P. Alivisatos, *Nature* 370, 354 **(1994)**.
6. W. C. W. Chen and S. Nie, *Science* 281, 2016 **(1998)**.
7. G. P. Mitchell, C. A. Mirkin, and R. L. Letsinger, *J. Am. Chem. Soc.* 121, 8122 **(1999)**.
8. X. G. Peng, L. Manna, W. D. Yang et al., *Nature* 404, 59 **(2000)**.
9. M. Dahan, T. Laurence, F. Pinaud, D. S. Chemla, A. P. Alivisatos, M. Sauer, and S. Weiss, *Opt. Lett.* 26, 825 **(2001)**.
10. D. Gerion, F. Pinaud, S. C. Williams, W. J. Parak, D. Zanchet, S. Weiss, and A. P. Alivisatos, *J. Phys. Chem. B* 105, 8861 **(2001)**.
11. B. P. Zhang, T. Yasuda, Y. Segawa, H. Yaguchi, K. Onabe, E. Edamatsu, and T. Itoh, *Appl. Phys. Lett.* 70, 2413 **(1997)**.
12. M. C. Liao, Y. H. Chang, Y. F. Chen, J. W. Hsu, J. M. Lin, and W. C. Chou, *Appl. Phys. Lett.* 70, 2256 **(1997)**.
13. E. D. Bourret-Courchense, *Appl. Phys. Lett.* 68, 2418 **(1996)**.
14. H. Saloniemi, T. Kanniainen, M. Riatala, M. Leskela, and R. Lappalainen, *J. Mater. Chem.* 8, 651 **(1998)**.
15. Y. D. Li, Y. Ding, Y. T. Qian, Y. Zhang, and L. Yang, *Inorg. Chem.* 37, 2844 **(1998)**.
16. C. Wang, W. X. Zhang, Y. Ding, Y. T. Qian, Y. Li, and G. E. Zhou, *Chem. Mater.* 10, 2301 **(1998)**.
17. C. N. R. Rao, A. Govindaraj, F. Leonard Deepak, and N. A. Gunari, *Appl. Phys. Lett.* 78, 1853 **(2001)**.
18. R. Sathyamoorthy, V. Manjuladevi, P. Sudhagar, S. Senthilarasu, and U. Pal, *J. Mater. Chem. Phys.*, submitted.
19. M. Skyllas and K. B. Miller, *J. Electrochem. Soc.* 127, 8569 **(1980)**.
20. M. Cardona, K. L. Shaklee, and F. H. Pollak, *Phys. Rev.* 154, 696 **(1967)**.
21. U. Pal, D. Samanta, S. Ghorai, and A. K. Chaudhuri, *J. Appl. Phys.* 74, 6368 **(1993)**.
22. M. Normal, D. J. Norris, M. Kuno, and M. G. Bawendi, *Phys. Rev. Lett.* 75, 3728 **(1995)**.
23. M. S. Shaalan and R. Müller, *Sol. Cells* 28, 185 **(1990)**.
24. C. B. Murray, D. J. Norris, and M. G. Bawendi, *J. Am. Chem. Soc.* 115, 8706 **(1993)**.
25. R. B. Kale, S. D. Sartale, B. K. Chougule, and C. D. Lokhande, *Semicond. Sci. Technol.* 19, 980 **(2004)**.
26. R. B. Kale and C. D. Lokhande, *Semicond. Sci. Technol.* 20, 1 **(2005)**.

Received: 6 December 2007. Accepted: 18 May 2008.